

Article

In-Vitro Cell Response to Strontium/Magnesium-Doped Calcium Phosphate Nanoparticles

Kathrin Kostka , Shabnam Hosseini and Matthias Eppele * 

Inorganic Chemistry and Centre for Nanointegration Duisburg-Essen (CENIDE), University of Duisburg-Essen, 45117 Essen, Germany

* Correspondence: matthias.eppele@uni-due.de

Abstract: Calcium phosphate nanoparticles are highly biocompatible and biodegradable in bone regeneration. On the other hand, strontium and magnesium enhance the formation of bone. The substitution of calcium by strontium and magnesium is an efficient way to improve the biological properties of calcium phosphate-based biomaterials. Strontium-doped calcium phosphate nanoparticles and magnesium-doped calcium phosphate nanoparticles with degrees of cation substitution of 5, 10, 15, and 20 mol% with respect to calcium were prepared by precipitation, followed by surface functionalization with polyethyleneimine (PEI, cationic) or carboxymethylcellulose (CMC, anionic). The nanoparticles were characterized by dynamic light scattering (DLS), zeta potential measurement, scanning electron microscopy (SEM), atomic absorption spectrometry (AAS), energy dispersive X-ray analysis (EDX), and X-ray powder diffraction (XRD). The particles were approximately spherical (diameter 40–70 nm). The addition of magnesium and strontium considerably decreased the internal crystallinity, i.e., the doped particles were almost X-ray amorphous. The cell-biological effects were assessed on three different cell lines, i.e., HeLa cells, MG63 cells, and MC3T3 cells. Cell viability tests (MTT) showed a low cytotoxicity, the alkaline phosphatase (ALP) activity was strongly increased, and the nanoparticles were taken up well by the three cell lines.

Keywords: bone regeneration; calcium phosphate; nanoparticles; strontium; magnesium



Citation: Kostka, K.; Hosseini, S.; Eppele, M. In-Vitro Cell Response to Strontium/Magnesium-Doped Calcium Phosphate Nanoparticles. *Micro* **2023**, *3*, 156–171. <https://doi.org/10.3390/micro3010012>

Academic Editor: Carlo Santulli

Received: 5 January 2023

Revised: 20 January 2023

Accepted: 25 January 2023

Published: 1 February 2023



Copyright: © 2023 by the authors. Licensee MDPI, Basel, Switzerland. This article is an open access article distributed under the terms and conditions of the Creative Commons Attribution (CC BY) license (<https://creativecommons.org/licenses/by/4.0/>).

1. Introduction

Bone is an inorganic–bioorganic composite material consisting mainly of collagen and calcium phosphate [1,2]. Calcium phosphate nanoparticles that occur as hydroxyapatite constitute the inorganic basis of this biomineralized hard tissue, i.e., mammalian bone [3,4]. As they are inherently biocompatible and biodegradable [5], they have been extensively applied in the therapeutic delivery of drugs and biomolecules [1,6–9]. In the form of pastes and bone cements, calcium phosphate nanoparticles have been used for the repair of bone defects [9,10]. A bioactive coating of calcium phosphate nanoparticles with DNA and/or siRNA has been shown to induce bone formation (by transfection with DNA [11,12]) and to downregulate inflammatory proteins (by gene silencing with siRNA [13]).

The functionalization with drugs or biomolecules leads to a regulatory classification of a biomedical tool as a drug, which considerably complicates and prolongates its approval for clinical application [14–16]. For instance, medical devices that make use of nucleic acids or genes fall under the category of advanced therapy medicinal products (ATMPs) [17]. An alternative is the modification of the well-known and approved calcium phosphate (even as food additive [18]) with inorganic ions which enhance its properties but do not make it a drug. In the last decade, the doping of hydroxyapatite with foreign ions has been shown to improve the cell response and the biocompatibility of calcium phosphates [19–21]. As substituting ions, carbonate (leading to carbonated apatite [22,23]) and silicate [24–26] have been introduced to enhance bioactivity in bone contact. Silver [10,27,28], copper [29,30], and zinc [31,32] have been substituted for calcium to induce an antibacterial action (Ag and

Cu) and to enhance bone growth (Zn). The most important cation that replaces calcium in biologically occurring apatite is magnesium, which also plays an essential role in bone metabolism. In bone metabolism, magnesium influences the activities of bone-forming osteoblasts and bone-degrading osteoclasts [33], in addition to exerting a number of other important metabolic functions inside the cells [34,35]. Consequently, it has been added to calcium phosphate-based bioceramics to enhance bone formation [10,36].

Strontium plays an important role in bone formation. The beneficial use of strontium in bone therapies has been reported [37,38]. Strontium has been proposed to constrain osteoporosis. It promotes osteoblast function and inhibits osteoclast performance in vitro [39]. Strontium ranelate (a water-soluble drug) was used to treat osteoporosis after menopause [40,41], but was removed from the market approximately ten years ago due to adverse side reactions [42]. However, strontium has been proposed as an additive to calcium phosphate-based biomaterials for bone reconstruction [10,36,39,43–50]. There, it is only slowly mobilized and does not cause the side reactions of a strontium salt after ingestion. The addition of strontium as a component of calcium phosphate nanoparticles should preserve its positive action while avoiding the negative effects of strontium ranelate.

Here, we demonstrate how colloiddally stabilized calcium phosphate nanoparticles can be doped with different amounts of magnesium and strontium for their potential application in bone regeneration. Such nanoparticles could act as transporters of these beneficial ions into cells, e.g., after incorporation into a calcium phosphate cement or a calcium phosphate paste. Nanoparticles are mobilized and degraded more easily than sintered calcium phosphate ceramics [51], but are far less mobile than small molecules or ions [52]. The cell-biological effects of the nanoparticles are tested with three different cell lines: human cervix carcinoma cells (HeLa) as the standard cell line, human osteosarcoma cells (MG 63), and an osteoblast mouse precursor cell line derived from calvaria (MC3T3) as models for bone cells.

2. Materials and Methods

2.1. Reagents

Poly(ethyleneimine) (PEI, branched, $M_w = 25$ kDa) was obtained from Sigma-Aldrich (now Merck, Darmstadt, Germany). Fluorescent rhodamine-labelled PEI (PEI^{Rh}, branched, $M_w = 25$ kDa) was obtained from Surflay (Berlin, Germany). Calcium lactate (p.a.; Merck), diammonium hydrogen phosphate (p.a.; Merck), strontium nitrate (Merck), magnesium nitrate hexahydrate (Merck), trehalose (>98%; VWR Life Science, Darmstadt, Germany), and aqueous ammonia solution (30–33%, Carl Roth, Karlsruhe, Germany) were used as obtained. Sodium carboxymethyl cellulose (CMC, $M_w = 90$ kDa) was obtained from Sigma-Aldrich. Carboxymethylcellulose was conjugated with 6-aminofluorescein (CMC-F), as reported earlier [53].

2.2. Instruments

Scanning electron microscopy (SEM) was performed with an ESEM Quanta 400 instrument (FEI, Hillsboro, OR, USA) with gold/palladium-sputtered samples, combined with energy-dispersive X-ray spectroscopy (EDX; detector type: SUTW-sapphire, resolution: 128.81, Lsec: 50). The samples were drop-cast onto the sample holder and dried in the air before sputtering (in the absence of trehalose).

Dynamic light scattering (DLS) and zeta potential determinations were performed with a Zetasizer Nanoseries instrument (Malvern Panalytical, Malvern, UK; Malvern Nano-ZS, laser wavelength $\lambda = 532$ nm), using the Smoluchowski approximation and taking the data from the Malvern software without further correction. The particle size data refer to scattering intensity distributions (z-average). The particles were dispersed in neutral water at a concentration of approximately 1 mg mL^{-1} .

X-ray powder diffraction (XRD) was performed using a Bruker D8 system (Bruker, Billerica, MA, USA) with Cu $K\alpha$ radiation ($\lambda = 1.54 \text{ \AA}$) on silicon, single-crystal sample

holders (range 5–90 °2 Θ ; step size 0.01 °2 Θ ; count time 0.6 s; nickel filter). The particles were drop-cast onto the sample holder and dried in the air (in the absence of trehalose).

Confocal laser scanning microscopy (CLSM) was performed with an SP8 Falcon (Leica, Wetzlar, Germany) instrument with a 63 \times water objective. The laser wavelength was $\lambda = 405$ nm for Hoechst33342 excitation (emission: 440–480 nm), $\lambda = 488$ nm for CMC-F excitation (emission: 510–540 nm), $\lambda = 488$ nm for AlexaFluor[®] 488-phalloidin excitation (emission: 510–540 nm), $\lambda = 647$ nm for AlexaFluor[®] 647-phalloidin excitation (emission: 680–720 nm), and $\lambda = 590$ nm for rhodamine excitation (emission: 610 nm).

Centrifugation for particle purification was performed with a Heraeus Fresco 21 instrument (Thermo Fisher Scientific, Waltham, MA, USA). The cell viability was analyzed with the MTT test by spectrophotometric analysis with a Multi-scan FC instrument (Thermo Fisher Scientific). Freeze-drying was performed with an Alpha 2-4 LSC instrument (Martin Christ, Osterode am Harz, Germany).

2.3. Synthesis of Strontium-Doped Calcium Phosphate Nanoparticles

According to earlier reported protocols, strontium-doped calcium phosphate nanoparticles were prepared in the same way as undoped calcium phosphate nanoparticles [54]. The molar contents of strontium with respect to calcium were 5, 10, 15, and 20%. Strontium-free calcium phosphate nanoparticles were prepared as a control. The synthesis of the 5% strontium-doped calcium phosphate nanoparticles is described in the following; the other syntheses were performed accordingly. Aqueous solutions of 1.75 mL of calcium lactate pentahydrate (4.54 mM, pH 10.0), 1.75 mL of strontium nitrate (0.24 mM, pH 10.0), and 3.5 mL of diammonium hydrogen phosphate (2.77 mM, pH 10.0) were pumped simultaneously with a peristaltic pump at 5 mL min⁻¹ each into a round-bottom flask and stirred for 5 min. For colloidal stabilization, the formed particle dispersion was taken with a syringe and rapidly injected into 1.5 mL of a PEI solution (2 g L⁻¹), followed by stirring for another 20 min. The particles were isolated by 15 min of centrifugation at 21,100 \times g, followed by redispersion in water or cell-culture medium under gentle ultrasonication. To obtain fluorescent particles, 5% of PEI^{Rh} was added to the PEI solution before the synthesis. Finally, 20 mg of the cryoprotectant trehalose was added to 1 mL of the nanoparticle dispersion before freeze-drying.

2.4. Synthesis of Magnesium-Doped Calcium Phosphate Nanoparticles

Magnesium-doped calcium phosphate nanoparticles were prepared in the same manner as the strontium-doped nanoparticles, with molar contents of magnesium of 5, 10, 15, and 20%. Stabilization of the particles was performed either with 1.5 mL PEI solution (as described above) or with 1.5 mL of CMC solution (2 g L⁻¹). To prepare fluorescent CMC-coated nanoparticles, carboxymethylcellulose (CMC), labelled with 6-aminofluoresceine [53], was used (CMC-F). Finally, 20 mg of the cryoprotectant trehalose was added to 1 mL of the nanoparticle dispersion before freeze-drying.

2.5. Cell Culture Studies

Freeze-dried nanoparticles (including trehalose) were redispersed in the cell culture medium (DMEM) under gentle vortexing. All given concentrations refer to the combined mass of trehalose and nanoparticles. The cell culture studies were carried out with human cervix carcinoma cells (HeLa), human osteosarcoma cells (MG 63), and an osteoblast mouse precursor cell line derived from calvaria (MC3T3). The cells were cultured in Dulbecco's modified Eagle's medium (DMEM), supplemented with 10% fetal bovine serum (FBS, Gibco), 100 U mL⁻¹ of penicillin, and 100 U mL⁻¹ of streptomycin at 37 °C in a humidified atmosphere with 5% CO₂. An amount of 3 mg of the freeze-dried nanoparticles was dispersed in 500 μ L of DMEM prior to the addition to the cells.

The cytotoxicity was assessed with a 3-(4,5-dimethylthiazol-2-yl)-2,5-diphenyltetrazolium bromide (MTT) cytotoxicity assay. The cells were trypsinized and seeded in a 24-well culture dish with 2.5 \times 10⁴ cells per well in 500 μ L of cell culture medium 24 h prior

to the experiments. An amount of 100 μL of the nanoparticle dispersion in DMEM was added to the cells, which were then incubated for 24 h. Afterwards, the cells were washed three times with 500 μL of PBS each and incubated with 300 μL of MTT solution (1 g L^{-1}) for 1 h at 37°C . The MTT solution was then replaced by 300 μL of DMSO, and the cells were incubated for another 30 min. Finally, sample triplicates of the DMSO solution were transferred to a 96-well plate (100 μL aliquots) for spectrophotometric analysis at 570 nm. The relative cell viability was calculated in comparison with a control group of untreated cells.

For the nanoparticle uptake studies, the cells were trypsinized and seeded in a glass bottom dish with 10^4 cells per well in 250 μL of cell culture medium 24 h prior to the experiment. The cells were then incubated for 24 h with 250 μL of the nanoparticle dispersion. The cells were washed three times with 300 μL of PBS to remove adherent nanoparticles. Finally, the cells were fixed with 100 μL of a 4% aqueous formaldehyde solution for 20 min at room temperature and washed again three times with 300 μL of PBS each. Prior to actin staining, the cells were permeabilized with 150 μL of 0.1% Triton X-100 for 5 min and washed twice with 300 μL of PBS each. For actin staining, the cells were incubated with 150 μL of a solution of $25 \mu\text{g mL}^{-1}$ of either AlexaFluor[®] 488-phalloidin or AlexaFluor[®] 647-phalloidin (Invitrogen, Karlsruhe, Germany) in PBS with 1% bovine serum albumin. They were then washed three times with 150 μL of PBS each. The cell nucleus was stained with 150 μL of a $10 \mu\text{g mL}^{-1}$ solution of Hoechst33342 (Life Technologies, Eugene, OR, USA) for 15 min. The cells were washed three times with 300 μL of PBS each and finally stored in 250 μL of PBS.

The alkaline phosphatase (ALP) activity was measured according to the manufacturer's instructions, using an Alkaline Phosphatase Assay Kit (Colorimetric; ab83369) (abcam, Cambridge, UK). HeLa cells were seeded in a 24-well plate at a density of 10,000 cells per well and incubated for 24 h. After removing the culture medium, the cells were treated with 500 μL of DMEM containing 100 μL (3 mg mL^{-1}) of dispersed nanoparticles. After 24 h of incubation, the cell medium was removed and the ALP activity was measured on days 7, 14 and 21 after incubation.

3. Results and Discussion

Three different series of doped nanoparticles were synthesized. The first group consisted of positively charged, strontium-doped calcium phosphate nanoparticles, stabilized with the cationic polyelectrolyte PEI. The second group consisted of positively charged, magnesium-doped calcium phosphate nanoparticles, stabilized with PEI. The third group consisted of negatively charged, magnesium-doped calcium phosphate, stabilized with the anionic polyelectrolyte CMC to elucidate the effect of the particle charge on the particle properties. Undoped calcium phosphate nanoparticles were prepared as a control, with both PEI and CMC functionalization. Figure 1 schematically shows the synthesis of the nanoparticles by rapid precipitation from water, followed by surface coating with a polyelectrolyte. The doped nanoparticles are denoted as the following, with respect to their composition and surface coating, e.g., (Ca/Sr)P/PEI^{Rh} 90:10 indicates a molar ratio of calcium to strontium of 90:10 and a surface coating with PEI^{Rh}.

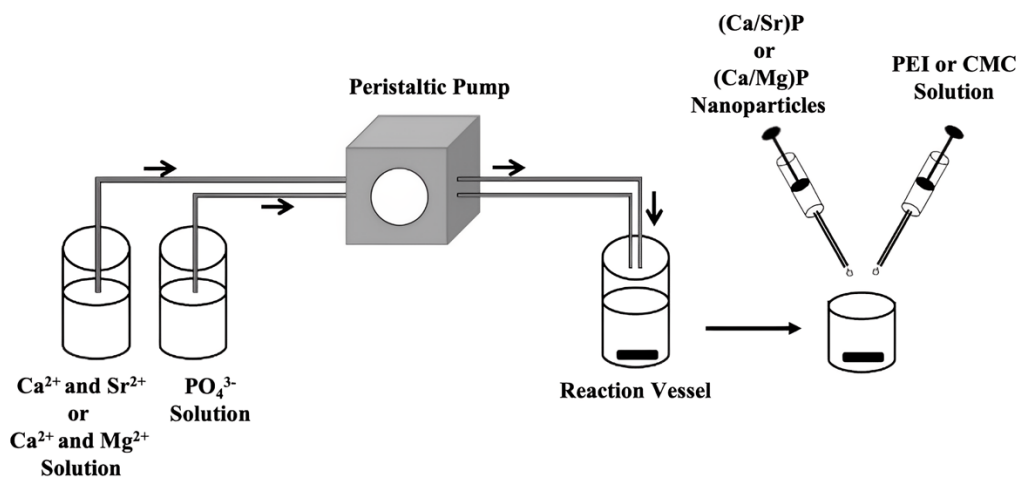


Figure 1. Schematic representation of the synthesis of the doped calcium phosphate nanoparticles. Aqueous solutions of the constituting ions were rapidly pumped into a reaction vessel for precipitation. An aliquot was then taken with a syringe and injected into solutions of either PEI or CMC to coat the particles' surfaces. This prevented particle growth and agglomeration.

After purification by centrifugation, washing, and redispersion, all nanoparticles were characterized by scanning electron microscopy (SEM), dynamic light scattering (DLS), atomic absorption spectroscopy (AAS), energy-dispersive X-ray spectroscopy (EDX), and X-ray powder diffraction (XRD). Figure 2 shows SEM images of all the prepared particles. Most particles were approximately spherical, with an average diameter of the solid core of approximately 40–70 nm, independent of the composition of the particles. The average particle size was determined manually by analyzing 100 to 200 particles per sample. Neither the ion substitution nor the surface coating had a significant effect on the particle size (see also Table 1).

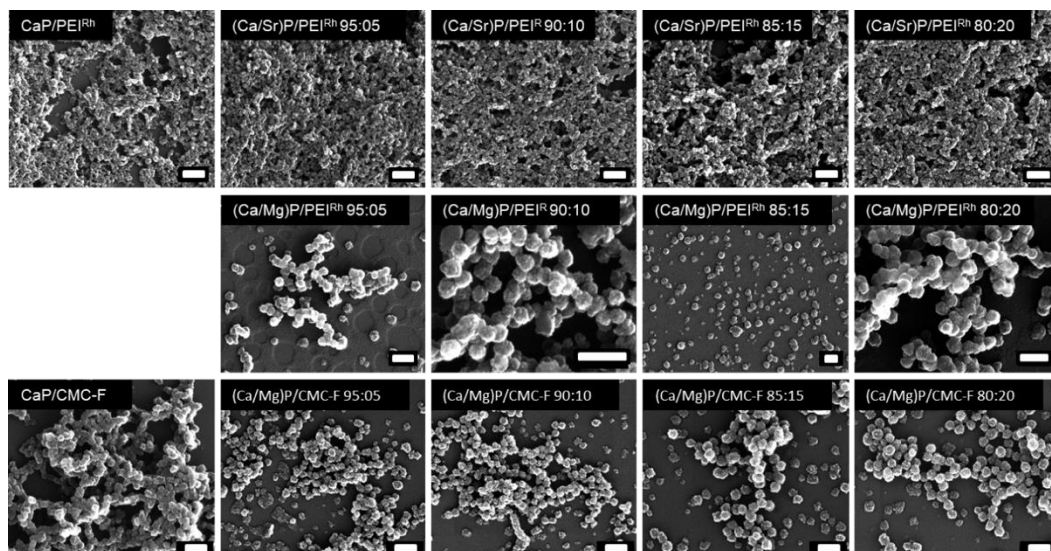


Figure 2. Scanning electron micrographs of undoped calcium phosphate nanoparticles and of strontium- or magnesium-doped calcium phosphate nanoparticles, stabilized and labelled with either PEI^{Rh} or CMC-F. All scalebars: 200 nm.

Table 1. Characterization of calcium phosphate-only nanoparticles as well as strontium- and magnesium-doped calcium phosphate nanoparticles, stabilized and labelled with either PEI^{Rh} or CMC-F. The errors in the molar ratios of the elements are estimated to be about 5% (relative) for each element (for AAS and EDX results). In general, the results by AAS and EDX show a good agreement with a particle composition close to the ratio of the ions during synthesis.

Sample	Hydrodynamic Diameter (DLS)/nm	Zeta Potential/mV	Solid Core Diameter (SEM)/nm	Molar Ratio Ca:Mg/Sr by AAS/mol%	Molar Ratio Ca:Mg/Sr by EDX/mol%
CaP/PEI ^{Rh}	105 ± 28	+11 ± 3	50 ± 12	100:0	100:0
(Ca/Sr)P/PEI ^{Rh} 95:5	80 ± 15	+9 ± 2	39 ± 07	94:6	95:5
(Ca/Sr)P/PEI ^{Rh} 90:10	100 ± 29	+8 ± 3	36 ± 05	92:8	91:9
(Ca/Sr)P/PEI ^{Rh} 85:15	90 ± 19	+9 ± 4	40 ± 08	84:16	84:16
(Ca/Sr)P/PEI ^{Rh} 80:20	102 ± 37	+11 ± 4	42 ± 06	81:19	82:18
(Ca/Mg)P/PEI ^{Rh} 95:5	105 ± 36	+5 ± 3	60 ± 18	93:7	93:7
(Ca/Mg)P/PEI ^{Rh} 90:10	95 ± 37	+8 ± 4	60 ± 15	89:11	89:11
(Ca/Mg)P/PEI ^{Rh} 85:15	95 ± 12	+8 ± 3	65 ± 20	84:16	83:17
(Ca/Mg)P/PEI ^{Rh} 80:20	90 ± 32	+15 ± 4	75 ± 16	81:19	82:18
CaP/CMC-F	125 ± 53	−17 ± 5	70 ± 11	100:0	100:0
(Ca/Mg)P/CMC-F 95:5	115 ± 48	−13 ± 3	65 ± 10	92:8	97:3
(Ca/Mg)P/CMC-F 90:10	105 ± 35	−19 ± 4	60 ± 10	93:7	90:10
(Ca/Mg)P/CMC-F 85:15	140 ± 33	−20 ± 5	75 ± 13	89:11	83:17
(Ca/Mg)P/CMC-F 80:20	140 ± 54	−18 ± 7	75 ± 14	86:14	79:21

Dynamic light scattering gave the particle size distributions in dispersion (Figure 3). The hydrodynamic diameter was between 80 and 140 nm. The particle diameters, which were slightly increased when compared to the SEM results indicate a moderate degree of agglomeration in all cases, but still a good dispersibility. The polydispersity index (PDI) was below 0.3 in all cases, indicating a stable dispersion. As expected, the particle charge, as expressed by the zeta potential, was positive for all PEI-coated nanoparticles and negative for all CMC-coated nanoparticles. The zeta potential is an important parameter for the interaction of nanoparticles with cells, especially for their uptake via endocytosis [55]. Usually, positively charged nanoparticles are taken up more easily by cells than negatively charged nanoparticles [56–58].

The ratio of dopant ions (strontium or magnesium) to calcium in the nanoparticles was determined by atomic absorption spectroscopy (AAS) and energy-dispersive X-ray spectroscopy (EDX). Within the experimental error of both methods, the composition of the nanoparticles was as expected, i.e., it corresponded well to the ratio of the ions applied during the synthesis. This shows that the precipitated nanoparticles had the same composition as in the ion solutions after mixing, i.e., there was no preferential, precipitation-specific solid formed. Figure 4 shows the results by EDX.

The internal structure of the nanoparticles was determined by X-ray powder diffraction. Figure 5 shows representative results. Notably, the undoped nanoparticles showed only the broad diffraction peaks of hydroxyapatite, Ca₅(PO₄)₃OH, as the most common calcium phosphate phase [59,60], indicating a poorly crystalline particle core. In contrast, both magnesium- and strontium-doped nanoparticles were almost X-ray amorphous, underscoring that the ionic substitution reduces the crystallinity of the calcium phosphate [59,61,62]. Strontium ions [63] and magnesium ions [64] are known to reduce the crystallinity of hydroxyapatite, as shown by in vitro crystallization studies. No foreign phases, such as strontium phosphate, Sr₃(PO₄)₂, or magnesium phosphate, Mg₃(PO₄)₂, were found, also in agreement with earlier reports [63,64]. Table 1 summarizes all analytical results.

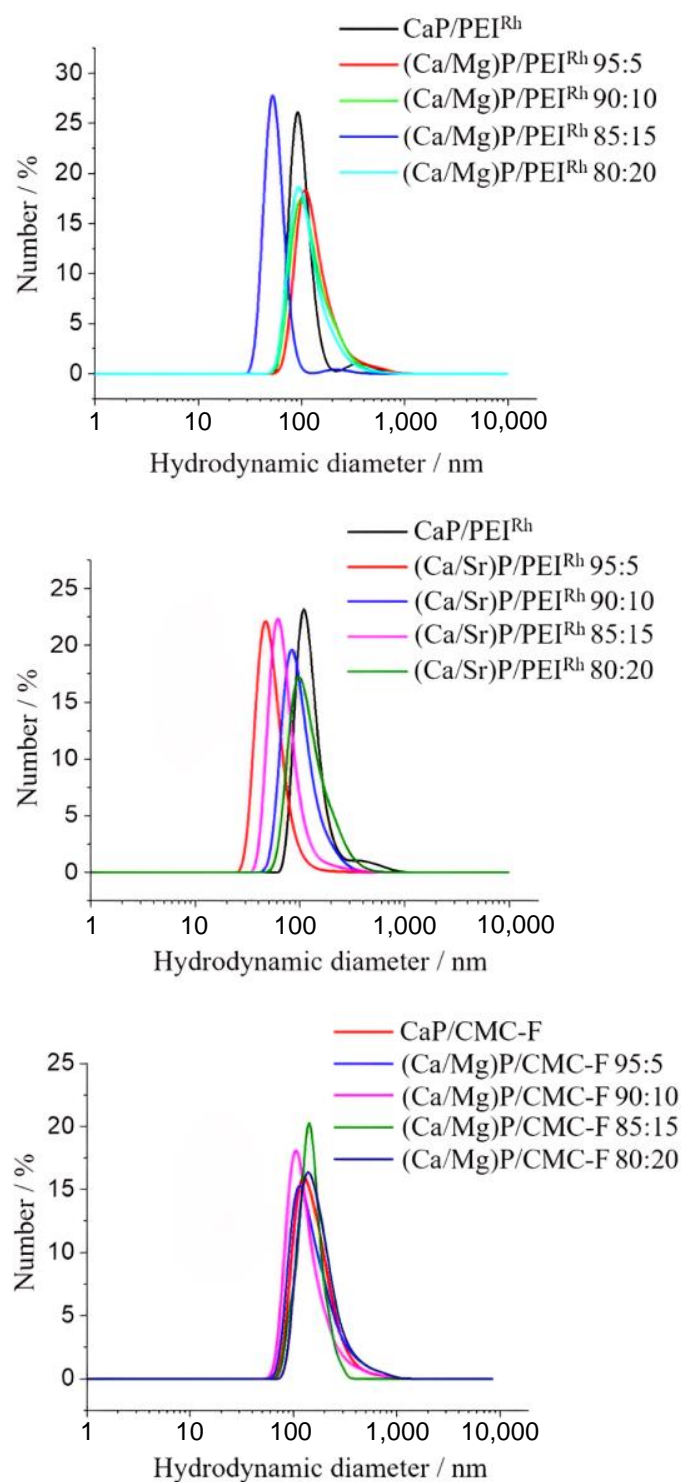


Figure 3. Dynamic light scattering results of undoped and magnesium- or strontium-doped calcium phosphate nanoparticles, stabilized and labelled with either PEI^{Rh} or CMC-F. Neither particle composition nor surface functionalization had a significant effect on the particle size distribution (represented by particle number distribution). No larger agglomerates were detectable.

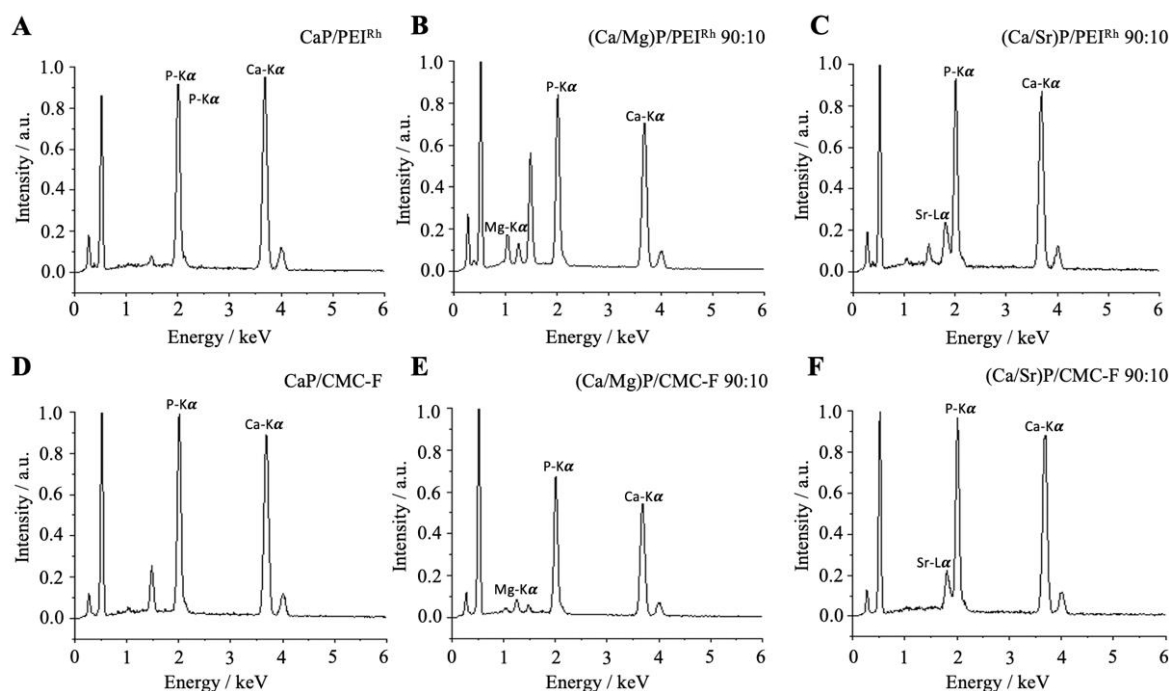


Figure 4. Representative energy-dispersive X-ray spectra (EDX) of calcium phosphate nanoparticles (A,D), magnesium-doped calcium phosphate nanoparticles (B,E); and strontium-doped calcium phosphate nanoparticles (C,F).

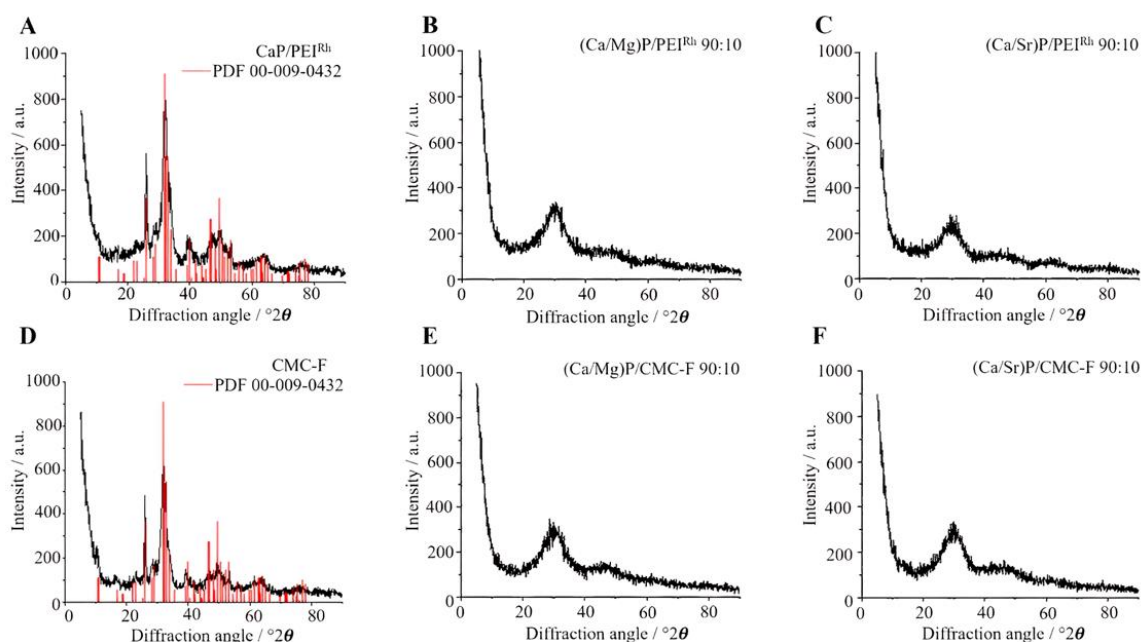


Figure 5. Representative X-ray powder diffractograms of calcium phosphate nanoparticles (A,D), magnesium-doped calcium phosphate nanoparticles (B,E); and strontium-doped calcium phosphate nanoparticles (C,F). The doping with magnesium or strontium considerably decreased the particle crystallinity. The diffraction peaks of the reference for hydroxyapatite (JCPDS No. 00-009-0432) are inserted as red bars. The increase in the diffraction intensity towards low angles is due to the primary (incoming) X-ray beam.

For any biological application, the particles must not be cytotoxic. Therefore, the viability of HeLa cells as model cell line was measured after 24 h incubation with nanoparticles to determine the cytotoxicity of the doped calcium phosphate nanoparticles (Figure 6). All

nanoparticles led to a high cell viability, regardless of the presence of the substituting ions. The slight decrease in cell viability may be ascribed to the moderately cytotoxic PEI [65,66] and an increase in the intracellular calcium concentration [67,68]. The presence of magnesium or strontium did not affect the cell viability. However, it should be noted that long-term incubation studies would be required for a full assessment of a potential cytotoxicity.

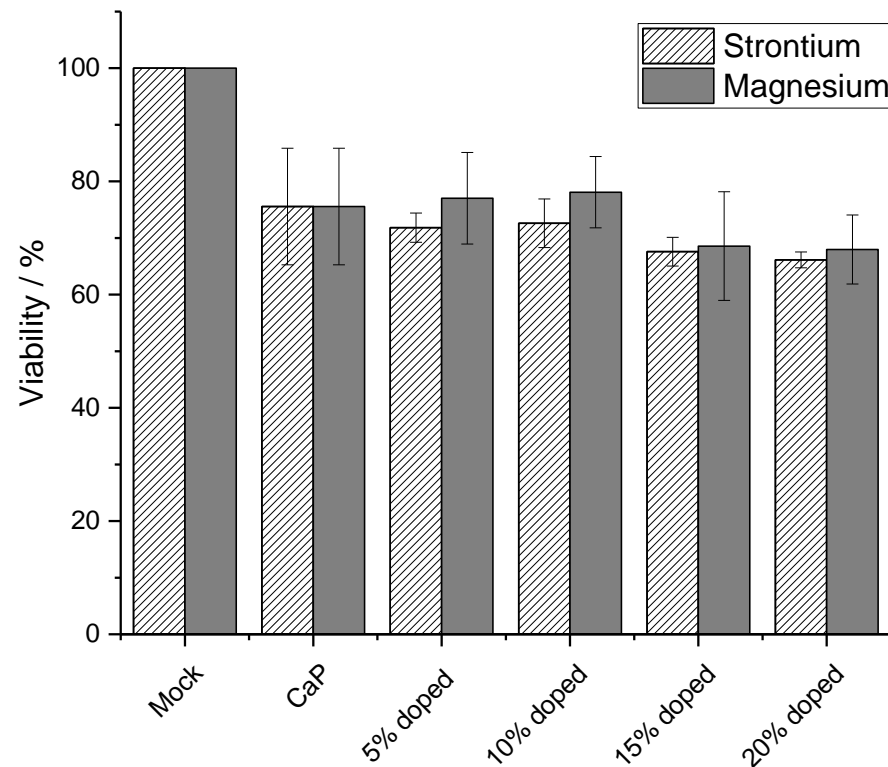


Figure 6. Viability of HeLa cells after 24 h incubation with undoped (CaP), strontium- and magnesium-doped calcium phosphate-PEI nanoparticles. Control: untreated cells (mock). $N = 3$ for each data point.

The uptake of the nanoparticles by the three different cell lines (HeLa, MG63, and MC3T3) was studied. HeLa cells are typical model cells. MG-63 cells are osteoblast-like cells [69], such as MC3T3 cells [70], i.e., they are well-suited to study the effect of calcium phosphate nanoparticles in bone contact. The uptake of fluorescently labelled particles was studied after 24 h of incubation time. Figure 7 shows confocal laser scanning microscopic images of HeLa cells. All types of particles were detected inside the cells, regardless of their charge or chemical composition. This is in line with earlier observations for calcium phosphate nanoparticles [6,71–73] and can be ascribed to endocytosis, as observed for many other types of nanoparticles [56,74–77].

Figure 8 shows the uptake of nanoparticles by MG-63 cells. As with the HeLa cells, all kinds of nanoparticles were taken up well by MG-63 cells.

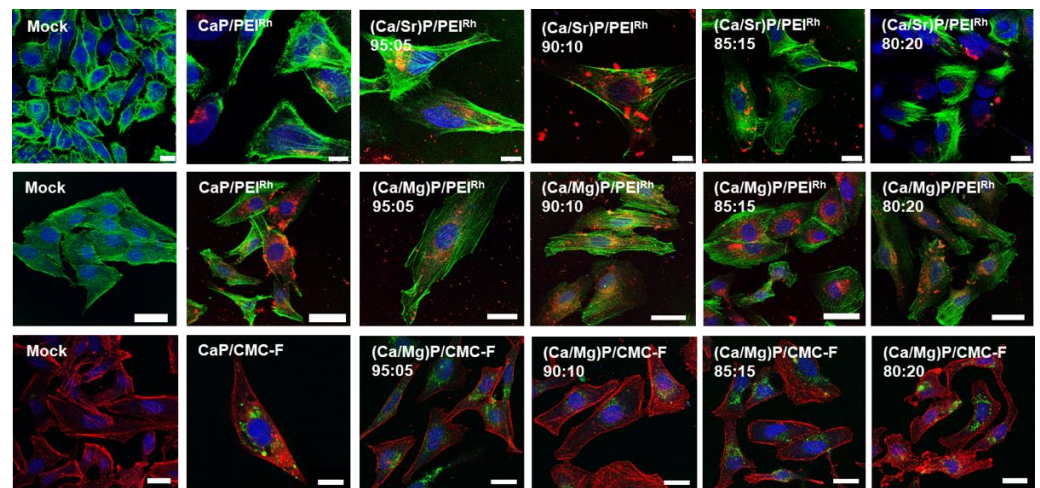


Figure 7. Confocal laser scanning microscopy of HeLa cells after incubation with nanoparticles for 24 h. Top row: Undoped calcium phosphate and strontium-doped calcium phosphate nanoparticles labelled with PEI^{Rh}. Blue: cell nucleus (Hoechst33342); green: cytoskeleton (actin with AlexaFluor[®]-488 phalloidin); and red: PEI^{Rh}-labelled nanoparticles. Middle row: calcium phosphate and magnesium-doped nanoparticles labelled with PEI^{Rh}. Blue: cell nucleus (Hoechst33342); green: cytoskeleton (actin with AlexaFluor[®]-488 phalloidin); and red: PEI^{Rh}-labelled nanoparticles. Bottom row: calcium phosphate and magnesium-doped nanoparticles labelled with CMC-F. Blue: cell nucleus (Hoechst33342); red: cytoskeleton (actin with AlexaFluor[®]-647 phalloidin); and green: CMC-F-labelled nanoparticles. Control: untreated cells (mock). Scale bars: 20 μ m.

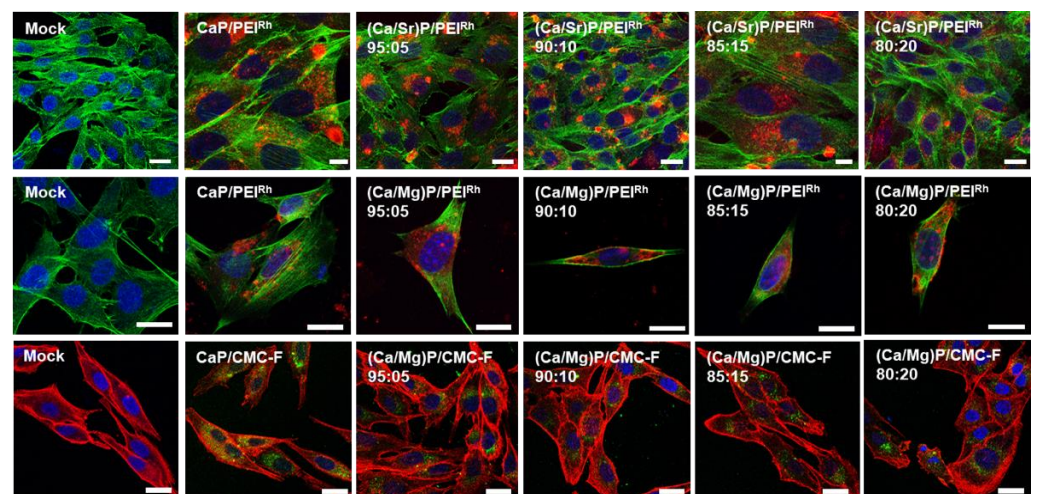


Figure 8. Confocal laser scanning microscopy of MG-63 cells after incubation with nanoparticles for 24 h. Top row: Undoped calcium phosphate and strontium-doped calcium phosphate nanoparticles labelled with PEI^{Rh}. Blue: cell nucleus (Hoechst33342); green: cytoskeleton (actin with AlexaFluor[®]-488 phalloidin); and red: PEI^{Rh}-labelled nanoparticles. Middle row: Calcium phosphate and magnesium-doped nanoparticles labelled with PEI^{Rh}. Blue: cell nucleus (Hoechst33342); green: Cytoskeleton (actin with AlexaFluor[®]-488 phalloidin); and red: PEI^{Rh}-labelled nanoparticles. Bottom row: Calcium phosphate and magnesium-doped nanoparticles labelled with CMC-F. Blue: Cell nucleus (Hoechst33342); red: Cytoskeleton (actin with AlexaFluor[®]-647 phalloidin); and green: CMC-F-labelled nanoparticles. Control: untreated cells (mock). Scale bars: 20 μ m.

Figure 9 shows the uptake results for MC3T3 cells, which also efficiently took up the nanoparticles. For the three cell lines, there was no significant difference between the uptake of strontium- or magnesium-doped calcium phosphate nanoparticles and undoped calcium phosphate nanoparticles. The nanoparticle charge also did not significantly in-

fluence the uptake. The nanoparticles were found throughout the cells, with no specific intracellular localization.

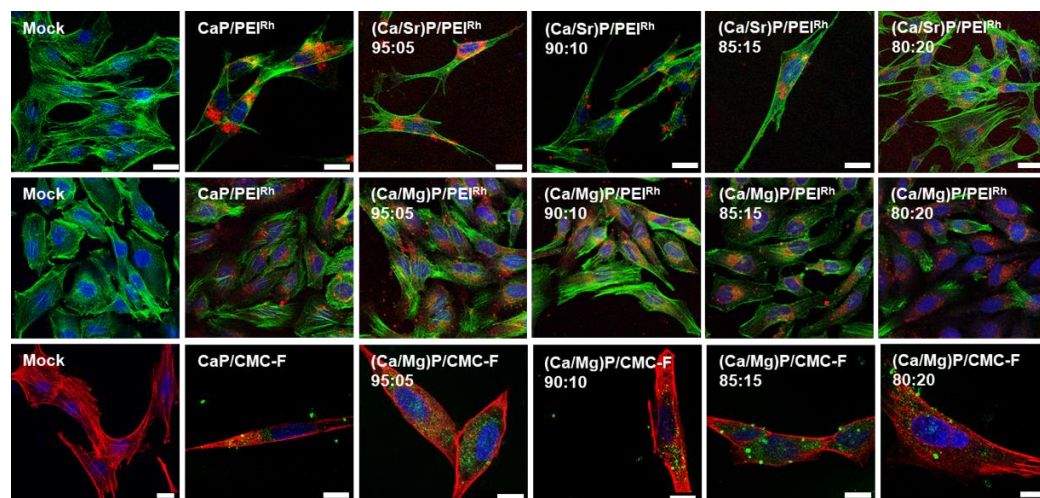


Figure 9. Confocal laser scanning microscopy of MC3T3 cells after incubation with nanoparticles for 24 h. Top row: Undoped calcium phosphate and strontium-doped calcium phosphate nanoparticles labelled with PEI^{Rh}. Blue: Cell nucleus (Hoechst33342); green: Cytoskeleton (actin with AlexaFluor[®]-488 phalloidin); red: PEI^{Rh}-labelled nanoparticles. Middle row: Calcium phosphate and magnesium-doped nanoparticles labelled with PEI^{Rh}. Blue: Cell nucleus (Hoechst33342); green: Cytoskeleton (actin with AlexaFluor[®]-488 phalloidin); red: PEI^{Rh}-labelled nanoparticles. Bottom row: Calcium phosphate and magnesium-doped nanoparticles labelled with CMC-F. Blue: Cell nucleus (Hoechst33342); red: Cytoskeleton (actin with AlexaFluor[®]-647 phalloidin); green: CMC-F-labelled nanoparticles. Control: Untreated cells (Mock). Scale bars: 20 μ m.

As a final marker for the cell-biological effect of doped calcium phosphate nanoparticles, we studied the activity of alkaline phosphatase (ALP). Alkaline phosphatase (ALP) plays a crucial role in bone formation as well as osteoid mineralization, in which it is involved as an enzyme in osteoblasts. Its main function is to provide inorganic phosphate for the synthesis of hydroxyapatite bone mineral. Another task is the hydrolysis of inorganic pyrophosphate, which serves as a mineralization inhibitor [78,79]. Figure 10 shows the activity of ALP in HeLa cells after 7, 14, and 21 days.

Calcium phosphate nanoparticles were used as control. In general, the presence of calcium phosphate nanoparticles strongly enhanced the ALP activity, increasingly so with a longer incubation time, in conclusion with the earlier reported data [80]. The doping with either strontium or magnesium resulted in a moderate additional increase of low statistical significance. The increase of ALP activity with the dopant concentration, either magnesium or strontium, was not statistically significant.

Our results are well in line with earlier work on the interaction of calcium phosphate nanoparticles with cells [6,81–84]. Usually, these particles are easily taken up by cells and do not induce a cytotoxicity unless applied at high dose [5]. The delivery of strontium and magnesium in nanoparticulate form enhances the availability of these ions to cells and could further enhance the therapeutic potential of calcium phosphate nanoparticles, e.g., as component in calcium phosphate cements for the treatment of bone defects [10,46,49,85–87].

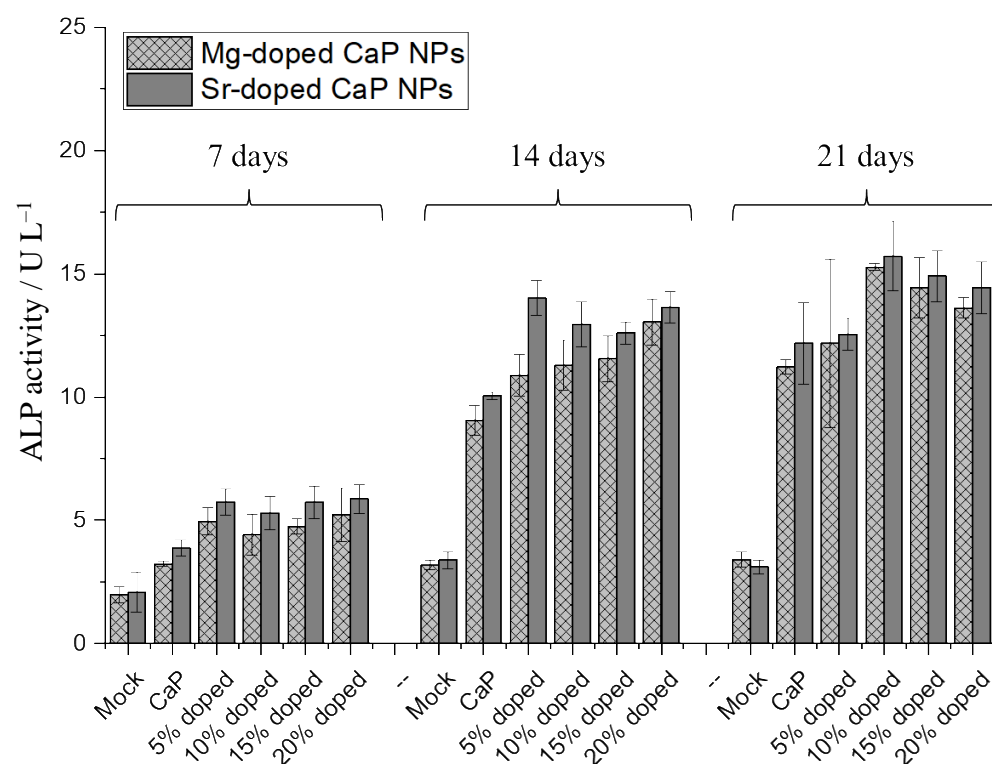


Figure 10. Alkaline phosphatase (ALP) activity in HeLa cells treated with undoped and strontium- or magnesium-doped PEI-functionalized calcium phosphate nanoparticles, normalized to the total protein content, after 7, 14, and 21 days. $N = 3$ for each data point. Error bars represent standard deviations. Control: untreated cells (mock).

4. Conclusions

A method to prepare uniform and spherical strontium- or magnesium-doped calcium phosphate nanoparticles, colloidal stabilized with either polyethyleneimine (PEI) or carboxymethylcellulose (CMC), was developed. The content of strontium or magnesium in the doped calcium phosphate nanoparticles can be adjusted by the synthesis conditions, i.e., the ratio of the elements in solutions. Both magnesium and strontium were substituted stoichiometrically (5 to 20 mol%) as in the solutions during synthesis, indicating a good substitution into the hydroxyapatite lattice. However, the internal crystallinity of the calcium phosphate nanoparticles was strongly reduced by the presence of both magnesium and strontium. The nanoparticles were not cytotoxic and were taken up well by three different cell lines, i.e., HeLa, MG-63, and MC3T3 cells. The nanoparticle charge did not influence the uptake efficiency. The activity of alkaline phosphatase was significantly increased by the nanoparticles in general, and a doping with magnesium and strontium moderately enhanced this effect. Thus, doped calcium phosphate nanoparticles represent a promising way to introduce magnesium and strontium into cells to induce biological effects, especially in bone contact.

Author Contributions: Conceptualization, M.E.; methodology, M.E.; validation, S.H., K.K. and M.E.; formal analysis, S.H., K.K. and M.E.; investigation, S.H. and K.K.; resources, M.E.; data curation, S.H., K.K. and M.E.; writing—original draft preparation, S.H. and K.K.; writing—review and editing, M.E.; visualization, S.H. and K.K.; supervision, M.E.; project administration, M.E. All authors have read and agreed to the published version of the manuscript.

Funding: This research received no external funding.

Institutional Review Board Statement: Not applicable.

Informed Consent Statement: Not applicable.

Data Availability Statement: Data are available from the authors upon request.

Acknowledgments: We thank the Imaging Centre Campus Essen (ICCE), Centre for Medical Biotechnology (ZMB), and the University of Duisburg-Essen for access to the confocal laser scanning microscopes. We thank Robin Meya, Ursula Giebel, Oliver Wetzel, and Dietrich Tönnies for their experimental assistance with elemental analysis, scanning electron microscopy, and X-ray powder diffraction.

Conflicts of Interest: The authors declare no conflict of interest.

References

1. Dorozhkin, S.V. Functionalized calcium orthophosphates (CaPO₄) and their biomedical applications. *J. Mater. Chem. B* **2019**, *7*, 7471–7489. [[CrossRef](#)] [[PubMed](#)]
2. Lu, J.Y.; Yu, H.J.; Chen, C.Z. Biological properties of calcium phosphate biomaterials for bone repair: A review. *RSC Adv.* **2018**, *8*, 2015–2033. [[CrossRef](#)]
3. Arcos, D.; Boccaccini, A.R.; Bohner, M.; Diez-Perez, A.; Epple, M.; Gomez-Barrena, E.; Herrera, A.; Planell, J.A.; Rodriguez-Manas, L.; Vallet-Regi, M. The relevance of biomaterials to the prevention and treatment of osteoporosis. *Acta Biomater.* **2014**, *10*, 1793–1805. [[CrossRef](#)] [[PubMed](#)]
4. Zakaria, S.M.; Sharif Zein, S.H.; Othman, M.R.; Yang, F.; Jansen, J.A. Nanophase hydroxyapatite as a biomaterial in advanced hard tissue engineering: A review. *Tissue Eng. B* **2013**, *19*, 431–441. [[CrossRef](#)] [[PubMed](#)]
5. Epple, M. Review of potential health risks associated with nanoscopic calcium phosphate. *Acta Biomater.* **2018**, *77*, 1–14. [[CrossRef](#)]
6. Sokolova, V.; Epple, M. Biological and medical applications of calcium phosphate nanoparticles. *Chem. Eur. J.* **2021**, *27*, 7471–7488. [[CrossRef](#)]
7. Habraken, W.; Habibovic, P.; Epple, M.; Bohner, M. Calcium phosphates in biomedical applications: Materials for the future? *Mater. Today* **2016**, *19*, 69–87. [[CrossRef](#)]
8. Mostaghaci, B.; Loretz, B.; Lehr, C.M. Calcium phosphate system for gene delivery: Historical background and emerging opportunities. *Curr. Pharm. Des.* **2016**, *22*, 1529–1533. [[CrossRef](#)]
9. Liu, C.; He, H. *Developments and Applications of Calcium Phosphate Bone Cements*; Springer: Berlin, Germany, 2018.
10. Demirel, M.; Canakci, D.; Aydin, M. Morphological and antibacterial effects of silver, magnesium, silicon and strontium modified calcium phosphate bone cements prepared by the sol-gel method. *Adv. Appl. Ceram.* **2020**, *119*, 324–433. [[CrossRef](#)]
11. Tenkumo, T.; Vanegas Sáenz, J.R.; Nakamura, K.; Shimizu, Y.; Sokolova, V.; Epple, M.; Kamano, Y.; Egusa, H.; Sugaya, T.; Sasaki, K. Prolonged release of bone morphogenetic protein-2 in vivo by gene transfection with DNA-functionalized calcium phosphate nanoparticle-loaded collagen scaffolds. *Mater. Sci. Eng. C* **2018**, *92*, 172–183. [[CrossRef](#)]
12. Schlickewei, C.; Klatter, T.O.; Wildermuth, Y.; Laaff, G.; Rueger, J.M.; Ruesing, J.; Chernousova, S.; Lehmann, W.; Epple, M. A bioactive nano-calcium phosphate paste for in-situ transfection of BMP-7 and VEGF-A in a rabbit critical-size bone defect: Results of an in vivo study. *J. Mater. Sci. Mater. Med.* **2019**, *30*, 15. [[CrossRef](#)] [[PubMed](#)]
13. Tenkumo, T.; Rojas-Sánchez, L.; Vanegas Sáenz, J.R.; Ogawa, T.; Miyashita, M.; Yoda, N.; Prymak, O.; Sokolova, V.; Sasaki, K.; Epple, M. Reduction of inflammation in a chronic periodontitis model in rats by TNF- α gene silencing with a topically applied siRNA-loaded calcium phosphate paste. *Acta Biomater.* **2020**, *105*, 263–279. [[CrossRef](#)] [[PubMed](#)]
14. Van Norman, G.A. Update to drugs, devices, and the FDA: How recent legislative changes have impacted approval of new therapies. *JACC Basic Transl. Sci.* **2020**, *5*, 831–839. [[CrossRef](#)] [[PubMed](#)]
15. Van Norman, G.A. Drugs and devices: Comparison of European and U.S. approval processes. *JACC Basic Transl. Sci.* **2016**, *1*, 399–412. [[CrossRef](#)]
16. Van Norman, G.A. Drugs, Devices, and the FDA: Part 2: An overview of approval processes: FDA approval of medical devices. *JACC Basic Transl. Sci.* **2016**, *1*, 277–287. [[CrossRef](#)]
17. Ramalhinho, A.C.; Castelo-Branco, M. Preparation of an academic clinical trial. *Methods Mol. Biol.* **2021**, *2197*, 317–330.
18. Enax, J.; Meyer, F.; Schulze zur Wiesche, E.; Epple, M. On the application of calcium phosphate micro- and nanoparticles as food additive. *Nanomaterials* **2022**, *12*, 4075. [[CrossRef](#)]
19. Graziani, V.; Fosca, M.; Egorov, A.A.; Zobkov, Y.V.; Fedotov, A.Y.; Baranchikov, A.E.; Ortenzi, M.; Caminiti, R.; Komlev, V.S.; Rau, J.V. Zinc-releasing calcium phosphate cements for bone substitute materials. *Ceram. Int.* **2016**, *42*, 17310–17316. [[CrossRef](#)]
20. Khan, A.F.; Saleem, M.; Afzal, A.; Ali, A.; Khan, A.; Khan, A.R. Bioactive behavior of silicon substituted calcium phosphate based bioceramics for bone regeneration. *Mater. Sci. Eng. C* **2014**, *35*, 245–252. [[CrossRef](#)]
21. Yang, G.; Liu, J.; Li, F.; Pan, Z.; Ni, X.; Shen, Y.; Xu, H.; Huang, Q. Bioactive calcium sulfate/magnesium phosphate cement for bone substitute applications. *Mater. Sci. Eng. C* **2014**, *35*, 70–76. [[CrossRef](#)]
22. Habibovic, P.; Juhl, M.V.; Clyens, S.; Martinetti, R.; Dolcini, L.; Theilgaard, N.; Van Blitterswijk, C.A. Comparison of two carbonated apatite ceramics in vivo. *Acta Biomater.* **2010**, *6*, 2219–2226. [[CrossRef](#)] [[PubMed](#)]
23. Khairoun, I.; Magne, D.; Gauthier, O.; Boulter, J.M.; Aguado, E.; Daculsi, G.; Weiss, P. In vitro characterization and in vivo properties of a carbonated apatite bone cement. *J. Biomed. Mater. Res.* **2002**, *60*, 633–642. [[CrossRef](#)] [[PubMed](#)]
24. Thian, E.S.; Huang, J.; Best, S.M.; Barber, Z.H.; Bonfield, W. Silicon-substituted hydroxyapatite: The next generation of bioactive coatings. *Mater. Sci. Eng. C* **2007**, *27*, 251–256. [[CrossRef](#)]

25. Bohner, M. Silicon-substituted calcium phosphates—A critical view. *Biomaterials* **2009**, *30*, 6403–6406. [[CrossRef](#)] [[PubMed](#)]
26. Jones, J.R. Review of bioactive glass: From Hench to hybrids. *Acta Biomater.* **2013**, *9*, 4457–4486. [[CrossRef](#)]
27. Ivanova, A.A.; Surmenev, R.A.; Surmeneva, M.A.; Mukhametkaliyev, T.; Loza, K.; Prymak, O.; Epple, M. Hybrid biocomposite with a tunable antibacterial activity and bioactivity based on RF magnetron sputter deposited coating and silver nanoparticles. *Appl. Surf. Sci.* **2015**, *329*, 212–218. [[CrossRef](#)]
28. Ewald, A.; Hösel, D.; Patel, S.; Grover, L.M.; Barralet, J.E.; Gbureck, U. Silver-doped calcium phosphate cements with antimicrobial activity. *Acta Biomater.* **2011**, *7*, 4064–4070. [[CrossRef](#)]
29. Shimabukuro, M.; Hayashi, K.; Kishida, R.; Tsuchiya, A.; Ishikawa, K. Surface functionalization with copper endows carbonate apatite honeycomb scaffold with antibacterial, proangiogenic, and pro-osteogenic activities. *Biomater Adv.* **2022**, *135*, 212751. [[CrossRef](#)]
30. Ghosh, R.; Swart, O.; Westgate, S.; Miller, B.L.; Yates, M.Z. Antibacterial copper-hydroxyapatite composite coatings via electrochemical synthesis. *Langmuir* **2019**, *35*, 5957–5966. [[CrossRef](#)]
31. Vukomanovic, M.; Gazvoda, L.; Anicic, N.; Rubert, M.; Suvorov, D.; Müller, R.; Hofmann, S. Multi-doped apatite: Strontium, magnesium, gallium and zinc ions synergistically affect osteogenic stimulation in human mesenchymal cells important for bone tissue engineering. *Biomater Adv.* **2022**, *140*, 213051. [[CrossRef](#)]
32. Wang, X.; Ito, A.; Sogo, Y.; Li, X.; Oyane, A. Zinc-containing apatite layers on external fixation rods promoting cell activity. *Acta Biomater.* **2010**, *6*, 962–968. [[CrossRef](#)] [[PubMed](#)]
33. Iafisco, M.; Ruffini, A.; Adamiano, A.; Sprio, S.; Tampieri, A. Biomimetic magnesium–carbonate-apatite nanocrystals endowed with strontium ions as anti-osteoporotic trigger. *Mater. Sci. Eng. C* **2014**, *35*, 212–219. [[CrossRef](#)] [[PubMed](#)]
34. Maguire, M.E.; Cowan, J.A. Magnesium chemistry and biochemistry. *Biomaterials* **2002**, *15*, 203–210. [[CrossRef](#)] [[PubMed](#)]
35. Nabiyouni, M.; Ren, Y.; Bhaduri, S.B. Magnesium substitution in the structure of orthopedic nanoparticles: A comparison between amorphous magnesium phosphates, calcium magnesium phosphates, and hydroxyapatites. *Mater. Sci. Eng. C* **2015**, *52*, 11–17. [[CrossRef](#)]
36. He, F.; Luc, T.; Fang, X.; Li, Y.; Zuo, F.; Deng, X.; Ye, J. Effects of strontium amount on the mechanical strength and cell-biological performance of magnesium-strontium phosphate bioceramics for bone regeneration. *Mater. Sci. Eng. C* **2020**, *112*, 110892. [[CrossRef](#)]
37. Verberckmoes, S.C.; De Broe, M.E.; D’Haese, P.C. Dose-dependent effects of strontium on osteoblast function and mineralization. *Kidney Int.* **2003**, *64*, 534–543. [[CrossRef](#)]
38. Schrooten, I.; Behets, G.J.; Cabrera, W.E.; Vercauteren, S.R.; Lamberts, L.V.; Verberckmoes, S.C.; Bervoets, A.J.; Dams, G.; Goodman, W.G.; De Broe, M.E.; et al. Dose-dependent effects of strontium on bone of chronic renal failure rats. *Kidney Int.* **2003**, *63*, 927–935. [[CrossRef](#)]
39. Marx, D.; Yazdi, A.R.; Papini, M.; Towler, M. A review of the latest insights into the mechanism of action of strontium in bone. *Bone Rep.* **2020**, *12*, 100273. [[CrossRef](#)]
40. Caverzasio, J. Strontium ranelate promotes osteoblastic cell replication through at least two different mechanisms. *Bone* **2008**, *42*, 1131–1136. [[CrossRef](#)]
41. Fardellone, P.; Roux, C.; Fechtenbaum, J.; Kolta, S.; Kruse, H.P.; Sawicki, A.; Hoszowski, K.; Padrino, J.; Sorensen, O.; Reginster, J.Y.; et al. Strontium ranelate reduces the risk of vertebral fractures in osteoporotic postmenopausal women whatever the baseline vertebral fracture status. *Bone* **2005**, *36*, 403.
42. Pilmane, M.; Salma-Ancane, K.; Loca, D.; Locs, J.; Berzina-Cimdina, L. Strontium and strontium ranelate: Historical review of some of their functions. *Mater. Sci. Eng. C Mater. Biol. Appl.* **2017**, *78*, 1222–1230. [[CrossRef](#)] [[PubMed](#)]
43. Scalera, F.; Palazzo, B.; Barca, A.; Gervaso, F. Sintering of magnesium-strontium doped hydroxyapatite nanocrystals: Towards the production of 3D biomimetic bone scaffolds. *J. Biomed. Mater. Res. A* **2020**, *108*, 633–644. [[CrossRef](#)] [[PubMed](#)]
44. Khalifehzadeh, R.; Arami, H. DNA-templated strontium-doped calcium phosphate nanoparticles for gene delivery in bone cells. *ACS Biomater. Sci. Eng.* **2019**, *5*, 3201–3211. [[CrossRef](#)] [[PubMed](#)]
45. Panzavolta, S.; Torricelli, P.; Casolari, S.; Parrilli, A.; Fini, M.; Bigi, A. Strontium-substituted hydroxyapatite-gelatin biomimetic scaffolds modulate bone cell response. *Macromol. Biosci.* **2018**, *18*, e1800096. [[CrossRef](#)]
46. Lode, A.; Heiss, C.; Knapp, G.; Thomas, J.; Nies, B.; Gelinsky, M.; Schumacher, M. Strontium-modified premixed calcium phosphate cements for the therapy of osteoporotic bone defects. *Acta Biomater.* **2018**, *65*, 475–485. [[CrossRef](#)]
47. Kruppke, B.; Heinemann, C.; Gebert, A.; Rohnke, M.; Weiß, M.; Henß, A.; Wiesmann, H.P.; Hanke, T. Strontium substitution of gelatin modified calcium hydrogen phosphates as porous hard tissue substitutes. *J. Biomed. Mater. Res. A* **2021**, *109*, 722–732. [[CrossRef](#)]
48. Kruppke, B.; Ray, S.; Alt, V.; Rohnke, M.; Kern, C.; Kampschulte, M.; Heinemann, C.; Budak, M.; Adam, J.; Döhner, N.; et al. Gelatin-modified calcium/strontium hydrogen phosphates stimulate bone regeneration in osteoblast/osteoclast co-culture and in osteoporotic rat femur defects—In vitro to in vivo translation. *Molecules* **2020**, *25*, 5103. [[CrossRef](#)]
49. Wagner, A.S.; Schumacher, M.; Rohnke, M.; Glenske, K.; Gelinsky, M.; Arnhold, S.; Mazurek, S.; Wenisch, S. Incorporation of silicon into strontium modified calcium phosphate bone cements promotes osteoclastogenesis of human peripheral mononuclear blood cells. *Biomed. Mater.* **2019**, *14*, 025004. [[CrossRef](#)]

50. Kern, C.; Quade, M.; Ray, S.; Thomas, J.; Schumacher, M.; Gemming, T.; Gelinsky, M.; Alt, V.; Rohnke, M. Investigation of strontium transport and strontium quantification in cortical rat bone by time-of-flight secondary ion mass spectrometry. *J. R. Soc. Interface* **2019**, *16*, 20180638. [[CrossRef](#)]
51. Detsch, R.; Hagemeyer, D.; Neumann, M.; Schaefer, S.; Vortkamp, A.; Wuelling, M.; Ziegler, G.; Epple, M. The resorption of nanocrystalline calcium phosphates by osteoclast-like cells. *Acta Biomater.* **2010**, *6*, 3223–3233. [[CrossRef](#)]
52. Kollenda, S.A.; Klose, J.; Knuschke, T.; Sokolova, V.; Schmitz, J.; Staniszewska, M.; Costa, P.F.; Herrmann, K.; Westendorf, A.M.; Fendler, W.P.; et al. In vivo biodistribution of calcium phosphate nanoparticles after intravascular, intramuscular, intratumoral, and soft tissue administration in mice investigated by small animal PET/CT. *Acta Biomater.* **2020**, *109*, 244–253. [[CrossRef](#)] [[PubMed](#)]
53. Sokolova, V.; Rojas-Sanchez, L.; Bialas, N.; Schulze, N.; Epple, M. Calcium phosphate nanoparticle-mediated transfection in 2D and 3D mono- and co-culture cell models. *Acta Biomater.* **2019**, *84*, 391–401. [[CrossRef](#)] [[PubMed](#)]
54. Kozlova, D.; Chernousova, S.; Knuschke, T.; Buer, J.; Westendorf, A.M.; Epple, M. Cell targeting by antibody-functionalized calcium phosphate nanoparticles. *J. Mater. Chem.* **2012**, *22*, 396–404. [[CrossRef](#)]
55. Pelaz, B.; Alexiou, C.; Alvarez-Puebla, R.A.; Alves, F.; Andrews, A.M.; Ashraf, S.; Balogh, L.P.; Ballerini, L.; Bestetti, A.; Brendel, C.; et al. Diverse applications of nanomedicine. *ACS Nano* **2017**, *11*, 2313–2381. [[CrossRef](#)] [[PubMed](#)]
56. Patel, S.; Kim, J.; Herrera, M.; Mukherjee, A.; Kabanov, A.V.; Sahay, G. Brief update on endocytosis of nanomedicines. *Adv. Drug Deliv. Rev.* **2019**, *144*, 90–111. [[CrossRef](#)]
57. Foroozandeh, P.; Aziz, A.A. Insight into cellular uptake and intracellular trafficking of nanoparticles. *Nanoscale Res. Lett.* **2018**, *13*, 339. [[CrossRef](#)]
58. Zhang, S.; Gao, H.; Bao, G. Physical principles of nanoparticle cellular endocytosis. *ACS Nano* **2015**, *9*, 8655–8671. [[CrossRef](#)]
59. Dorozhkin, S.V. Nanosized and nanocrystalline calcium orthophosphates. *Acta Biomater.* **2010**, *6*, 715–734. [[CrossRef](#)]
60. Dorozhkin, S.V.; Epple, M. Biological and medical significance of calcium phosphates. *Angew. Chem. Int. Ed.* **2002**, *41*, 3130–3146. [[CrossRef](#)]
61. Dorozhkin, S.V. Amorphous calcium (ortho)phosphates. *Acta Biomater.* **2010**, *6*, 4457–4475. [[CrossRef](#)]
62. Dorozhkin, S.V. Synthetic amorphous calcium phosphates (ACPs): Preparation, structure, properties, and biomedical applications. *Biomater. Sci.* **2021**, *9*, 7748–7798. [[PubMed](#)]
63. Koutsoukos, P.G.; Nancollas, G.H. Influence of strontium ion on the crystallization of hydroxyapatite from aqueous solution. *J. Phys. Chem.* **1981**, *85*, 2403–2408. [[CrossRef](#)]
64. Bigi, A.; Falini, G.; Foresti, E.; Ripamonti, A.; Gazzano, M.; Roveri, N. Magnesium influence on hydroxyapatite crystallization. *J. Inorg. Biochem.* **1993**, *49*, 69–78. [[CrossRef](#)]
65. Paul, A.; Eun, C.J.; Song, J.M. Cytotoxicity mechanism of non-viral carriers polyethylenimine and poly-l-lysine using real time high-content cellular assay. *Polymer* **2014**, *55*, 5178–5188. [[CrossRef](#)]
66. Parhamifar, L.; Larsen, A.K.; Hunter, A.C.; Andresen, T.L.; Moghimi, S.M. Polycation cytotoxicity: A delicate matter for nucleic acid therapy—focus on polyethylenimine. *Soft Matter* **2010**, *6*, 4001–4009. [[CrossRef](#)]
67. Neumann, S.; Kovtun, A.; Dietzel, I.D.; Epple, M.; Heumann, R. The use of size-defined DNA-functionalized calcium phosphate nanoparticles to minimise intracellular calcium disturbance during transfection. *Biomaterials* **2009**, *30*, 6794–6802. [[CrossRef](#)]
68. Ewence, A.E.; Bootman, M.; Roderick, H.L.; Skepper, J.N.; McCarthy, G.; Epple, M.; Neumann, M.; Shanahan, C.M.; Proudfoot, D. Calcium phosphate crystals induce cell death in human vascular smooth muscle cells—A potential mechanism in atherosclerotic plaque destabilization. *Circ. Res.* **2008**, *103*, e28–e32. [[CrossRef](#)]
69. Miclau, T.; Edin, M.L.; Lester, G.E.; Lindsey, R.W.; Dahners, L.E. Bone toxicity of locally applied aminoglycosides. *J. Orthopaed. Trauma* **1995**, *9*, 401–406. [[CrossRef](#)]
70. Varanasi, V.G.; Saiz, E.; Loomer, P.M.; Ancheta, B.; Uritani, N.; Ho, S.P.; Tomsia, A.P.; Marshall, S.J.; Marshall, G.W. Enhanced osteocalcin expression by osteoblast-like cells (MC3T3-E1) exposed to bioactive coating glass (SiO₂-CaO-P₂O₅-MgO-K₂O-Na₂O system) ions. *Acta Biomater.* **2009**, *5*, 3536–3547. [[CrossRef](#)]
71. Sokolova, V.; Kozlova, D.; Knuschke, T.; Buer, J.; Westendorf, A.M.; Epple, M. Mechanism of the uptake of cationic and anionic calcium phosphate nanoparticles by cells. *Acta Biomater.* **2013**, *9*, 7527–7535. [[CrossRef](#)]
72. Rotan, O.; Severin, K.N.; Pöpsel, S.; Peetsch, A.; Merdanovic, M.; Ehrmann, M.; Epple, M. Uptake of the proteins HTRA1 and HTRA2 by cells mediated by calcium phosphate nanoparticles. *Beilstein J. Nanotechnol.* **2017**, *8*, 381–393. [[CrossRef](#)] [[PubMed](#)]
73. Kollenda, S.; Kopp, M.; Wens, J.; Koch, J.; Schulze, N.; Papadopoulos, C.; Pöhler, R.; Meyer, H.; Epple, M. A pH-sensitive fluorescent protein sensor to follow the pathway of calcium phosphate nanoparticles into cells. *Acta Biomater.* **2020**, *111*, 406–417. [[CrossRef](#)] [[PubMed](#)]
74. Beddoes, C.M.; Case, C.P.; Briscoe, W.H. Understanding nanoparticle cellular entry: A physicochemical perspective. *Adv. Coll. Interface Sci.* **2015**, *218*, 48–68. [[CrossRef](#)]
75. Canton, I.; Battaglia, G. Endocytosis at the nanoscale. *Chem. Soc. Rev.* **2012**, *41*, 2718–2739. [[CrossRef](#)] [[PubMed](#)]
76. Feliu, N.; Sun, X.; Alvarez Puebla, R.A.; Parak, W.J. Quantitative particle–cell interaction: Some basic physicochemical pitfalls. *Langmuir* **2017**, *33*, 6639–6646. [[CrossRef](#)] [[PubMed](#)]
77. Nazarenus, M.; Zhang, Q.; Soliman, M.G.; del Pino, P.; Pelaz, B.; Carregal-Romero, S.; Rejman, J.; Rothen-Rutishauser, B.; Clift, M.J.D.; Zellner, R.; et al. In vitro interaction of colloidal nanoparticles with mammalian cells: What have we learned thus far? *Beilstein J. Nanotechnol.* **2014**, *5*, 1477–1490. [[CrossRef](#)]

78. Wennberg, C.; Hessle, L.; Lundberg, P.; Mauro, S.; Narisawa, S.; Lerner, U.H.; Millan, J.L. Functional characterization of osteoblasts and osteoclasts from alkaline phosphatase knockout mice. *J. Bone Miner. Res.* **2000**, *15*, 1879–1888. [[CrossRef](#)]
79. Hessle, L.; Johnson, K.A.; Anderson, H.C.; Narisawa, S.; Sali, A.; Goding, J.W.; Terkeltaub, R.; Millan, J.L. Tissue-nonspecific alkaline phosphatase and plasma cell membrane glycoprotein-1 are central antagonistic regulators of bone mineralization. *Proc. Natl. Acad. Sci. USA* **2002**, *99*, 9445–9449. [[CrossRef](#)]
80. Ko, C.L.; Chen, J.C.; Tien, Y.C.; Hung, C.C.; Wang, J.C.; Chen, W.C. Osteoregenerative capacities of dicalcium phosphate-rich calcium phosphate bone cement. *J. Biomed. Mater. Res. A* **2015**, *103*, 203–210. [[CrossRef](#)]
81. Tsikourkitoudi, V.; Karlsson, J.; Merkl, P.; Loh, E.; Henriques-Normark, B.; Sotiriou, G.A. Flame-made calcium phosphate nanoparticles with high drug loading for delivery of biologics. *Molecules* **2020**, *25*, E1747. [[CrossRef](#)]
82. Rojas-Sanchez, L.; Loza, K.; Epple, M. Synthesis and intracellular tracing surface-functionalized calcium phosphate nanoparticles by super-resolution microscopy (STORM). *Materialia* **2020**, *12*, 100773. [[CrossRef](#)]
83. Khalifehzadeh, R.; Arami, H. Biodegradable calcium phosphate nanoparticles for cancer therapy. *Adv. Coll. Interface Sci.* **2020**, *279*, 102157. [[CrossRef](#)] [[PubMed](#)]
84. Uskoković, V.; Tang, S.; Nikolić, M.G.; Marković, S.; Wu, V.M. Calcium phosphate nanoparticles as intrinsic inorganic antimicrobials: In search of the key particle property. *Biointerphases* **2019**, *14*, 031001. [[CrossRef](#)] [[PubMed](#)]
85. Schumacher, M.; Lode, A.; Helth, A.; Gelinsky, M. A novel strontium(II)-modified calcium phosphate bone cement stimulates human-bone-marrow-derived mesenchymal stem cell proliferation and osteogenic differentiation in vitro. *Acta Biomater.* **2013**, *9*, 9547–9557. [[CrossRef](#)] [[PubMed](#)]
86. Pina, S.; Vieira, S.I.; Rego, P.; Torres, P.M.C.; da Cruz e Silva, O.A.B.; da Cruz e Silva, E.F.; Ferreira, J.M.F. Biological responses of brushite-forming Zn-and ZnSr-substituted β -Tricalcium phosphate bone cements. *Eur. Cells Mater.* **2010**, *20*, 162–177. [[CrossRef](#)]
87. Pina, S.; Torres, P.M.; Goetz-Neunhoffer, F.; Neubauer, J.; Ferreira, J.M.F. Newly developed Sr-substituted α -TCP bone cements. *Acta Biomater.* **2010**, *6*, 928–935. [[CrossRef](#)]

Disclaimer/Publisher's Note: The statements, opinions and data contained in all publications are solely those of the individual author(s) and contributor(s) and not of MDPI and/or the editor(s). MDPI and/or the editor(s) disclaim responsibility for any injury to people or property resulting from any ideas, methods, instructions or products referred to in the content.